Archaeological and Anthropological Sciences
https://doi.org/10.1007/s12520-019-00788-6

ORIGINAL PAPER

Micromorphological analysis of the deposits at the early pottery Xianrendong cave site, China: formation processes and site use in the Late Pleistocene

Ilaria Patania[1] · Paul Goldberg[2,3] · David Joel Cohen[4] · Xiaohong Wu[5] · Chi Zhang[5] · Ofer Bar-Yosef[1]

Received: 22 September 2016 / Accepted: 14 January 2019

Abstract

Excavations at the cave site of Xianrendong (Jiangxi Province, China) recovered the earliest known pottery (20/19,000 cal BP) in the world from a typical South China Upper Paleolithic chopper–chopping tool assemblage together with bone, antler, and shell tools. Here, we present the results of micromorphological and preliminary FTIR analysis of the deposits looking at high-resolution evidence of site formation processes, stratigraphic integrity, and spatial use of the site. The excavations in the cave can be divided into two areas, east and west. We demonstrate that the contexts of the micromorphological samples from both areas show negligible disturbances within the deposits, thus supporting the stratigraphic integrity of the radiocarbon samples used to date the pottery and site sequence. We also find differences in the formation processes between the east and west areas, including evidence of anthropogenic activities such as usage of hearths and dumping areas and differing geogenic inputs during the depositional history of each area. This study, the first of its kind for a Chinese Upper Paleolithic cave site, demonstrates the advantages of the systematic use of geoarchaeological methods (micromorphology and FTIR) for reconstructing human activities and site use and their environmental contexts.

Keywords Xianrendong cave · Late Pleistocene South China · Upper Paleolithic archeology · Micromorphology · FTIR analysis · Early pottery

Introduction

The Upper Paleolithic (or Late Paleolithic, as called in China) cave site of Xianrendong in Jiangxi province in southern China (Fig. 1) is well known for the discovery of the earliest pottery in the world, from hunter-gatherer contexts dating to 20,000 cal BP (Wu et al. 2012). This karst cave contains a sedimentological record spanning from ca. 29,000 to 9000 cal BP, with an occupational record of intermittent use of the cave by people for at least 16,000 years, beginning ca. 25,000 cal BP (Beijing and Jiangxi 2014; MacNeish 1999; Wu et al. 2012; Zhang 2002).

Excavations at Xianrendong reveal a typical South China Late Paleolithic material culture of core and flake tool technology with choppers and chopping tools, as well as some bone and shell tools (Jiangxi 1963). Within this assemblage, however, is also pottery (represented by a small number of sherds), first produced by foraging groups using the cave ca. 20,000 cal BP, and which today represents the earliest known example of pottery vessel production (Wu et al. 2012; Cohen 2013; Cohen et al. 2017). Excavations at the site were conducted over five seasons (1962, 1964, 1993, 1995, and 1999) in conjunction with the nearby cave of Diaotonghuan (Beijing and Jiangxi 2014, Jiangxi 1963, 1976; MacNeish and Libby 1995, 1999; Zhang 2002), but the complexity of the deposits and disagreements over the interpretation of the available

Electronic supplementary material The online version of this article (https://doi.org/10.1007/s12520-019-00788-6) contains supplementary material, which is available to authorized users.

✉ Ilaria Patania
ipatania@bu.edu

[1] Department of Anthropology, Harvard University, Cambridge, MA, USA

[2] CAS, SEALS, University of Wollongong, Wollongong, NSW 2522, Australia

[3] Institut für Naturwissenschaftliche Archäologie, Eberhard-Karls-Universität Tübingen, Rümelinstr. 23, 72070 Tübingen, Germany

[4] Department of Anthropology, National Taiwan University, Roosevelt Rd., Sec. 4, No. 1, Taipei 106, Taiwan

[5] School of Archaeology and Museology, Peking University, Beijing 100871, China

Published online: 23 February 2019

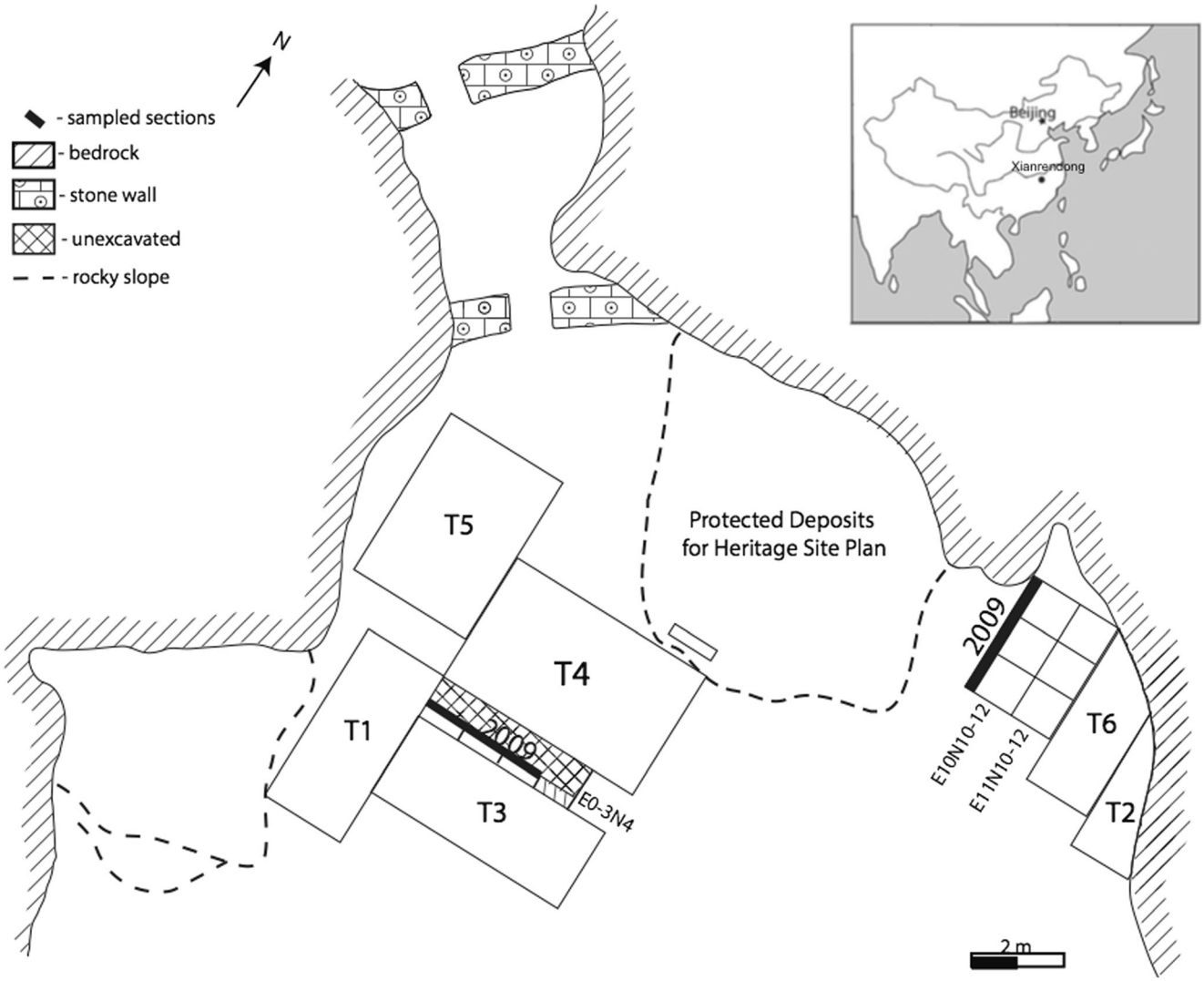

Fig. 1 Plan of Xianrendong Cave showing grid from the 1962–2009 excavations. Inset: location of Xianrendong in southern China (modified from Wu et al. 2012). Squares E0N4, E1N4, E2N4 show the 20 cm × 3 m area dug in the 1990s (MacNeish and Libby 1995, 1998). Dark lines indicate the "Western" and "Eastern" profiles re-exposed for micromorphological and radiocarbon sampling in 2009. The WP is in a corrected position from as originally plotted in Wu et al. (2012), Fig. 1. We also note that the absolute positions of the western and eastern groups of excavation units each may be off by perhaps 1 m. However, this does not impact the vertical integrity of the two profiles used in this study. Since we are not in possession of the original field notes, and to avoid further conjecture, we have left the plan unchanged. Future work at the cave should field check the units' positions and rectify the site plan, if needed

radiocarbon dates prevented a clear interpretation of the site's dating and usage. To resolve these issues, collaborative fieldwork in 2009 (with authors P.G., D.J.C., X.W., C.Z., and O.B.-Y. participating) reopened two earlier trenches (indicated in Fig. 1) to clarify chronological and site formation issues by employing a systematic sampling strategy for micromorphological analyses paired with radiocarbon dating (Wu et al. 2012). This paper provides new, more complete analyses of the micromorphological samples and the geoarchaeology from the site. These analyses allow us to see how the sedimentary history of the cave, and particularly episodes of flooding within parts of the cave, affected human occupation.

Xianrendong was discovered by Li Yanxian in 1961, with initial excavations of a large area of 41 m^2 (squares T1–T6; Fig. 1) in 1962 and 1964 (Jiangxi 1963, 1976). Further excavations in 1993 and 1995, aimed at investigating the origins of rice agriculture, by a Sino-American project led by Richard MacNeish, Chen Wenhua, and Peng Shifan opened an additional three units of 20 cm × 1 m each in the west (E0–2N4) and three 50 cm × 1 m units in the east (E11N10–12), with the goal of identifying the earliest presence and domestication sequence of rice in China (MacNeish and Libby 1995; MacNeish et al. 1998; Zhang 1999). In 1999, excavations of another 4.5 m^2 in the east (E11N10–12, E10N10–12) were directed by Peking University and the Jiangxi Provincial

Institute of Cultural Relics and Archeology (Wang et al. 2010; Zhang 1999). The determination of the dating of the early pottery proved problematic for the 1990s excavators (Cohen et al. 2017). Whereas AMS radiocarbon dates from bone and charcoal were acquired during both the 1995 and the 1999 excavations (MacNeish and Libby 1995; MacNeish et al. 1998; Beijing and Jiangxi 2014), many of the dates were rejected, as chronological interpretations were never tied to studies of the stratigraphy or site formation processes. MacNeish et al. (1998), MacNeish (1999) and Zhang (2002) instead relied on cross-dating to Jomon pottery in Japan to select radiocarbon dates of ca. 12,500 BP (uncalibrated) as the most plausible for the earliest pottery because they saw similarities between earliest Jomon pottery with that from Xianrendong. As a result, the excavators rejected the large number of radiocarbon dates dating before 12,500 BP (uncalibrated) that were stratigraphically associated with the pottery (Cohen et al. 2017; MacNeish et al. 1998; Wu et al. 2012; Zhang 2002).

The 2009 fieldwork was explicitly designed to re-date the stratigraphic contexts of the earliest pottery-containing layers at the site. With a large series of dating samples coupled with micromorphological analysis to test the stratigraphic integrity of their contexts, the 2009 operation was able to produce a new, secure chronology that placed the earliest pottery at ~ 20,000 cal BP (Wu et al. 2012). The dating results show that pottery production at the site begins shortly after the Last Glacial Maximum (defined now as Greenland Stadial 3, with dates of 27,540–23,340 cal BP; see Hughes et al. 2013; Hughes and Gibbard 2015) within a hunter-gatherer context and confirms that Xianrendong pottery is the earliest ceramic vessels not only in China but also known globally.

Here, we present detailed results of the geoarchaeological and micromorphological analysis of samples collected at Xianrendong in 2009 from both the eastern (EP) and western (WP) re-exposed profiles (Fig. 1). The purpose of this study is to reconstruct site formation processes, and we show how these were different in these separate areas of the cave. We also evaluate the integrity of the deposits paying special attention to the early pottery-containing layers in order to support the validity of the radiocarbon results by demonstrating there would have been no post-depositional movement of the radiocarbon samples.

Site setting and stratigraphy

Xianrendong Cave is situated in a karst landscape typical of South China, with limestone towers and peaks rising over alluvial valleys (Day and Tang 2004; Huang et al. 2013; Ford and Williams 1989; Waltham 2008; Zhang 1989; Zhu and Waltham 2004; Zhu et al. 2013). The cave entrance which faces southeast, is ca. 64 m above sea level (asl), and is only a few meters above the modern valley floor (Fig. 2), and filled with reddish brown silty clays. The entrance is 14.32 m wide and opens into a large chamber that narrows toward the back. Beyond a smaller, inner chamber, the cave system divides into five corridors that run N–S (Beijing and Jiangxi 2014). Wenxi Creek flows eastward toward the cave but turns abruptly northward without presently flowing in front of the mouth of the cave (Fig. 2). Two dams and a series of irrigation canals modify the modern course of this waterway in the area close to Dayuan village. From aerial photographs (Fig. 3) and topographic maps (Fig. 2), it appears that the channel once flowed through the valley south of Xianrendong but has since changed course.

The 2009 fieldwork reopened two trenches from earlier excavations: a western one from the 1993 excavation (north wall profile of E0–3N4, at a balk between it and T4), and an eastern one from the 1995–1999 excavations (west wall profile of E10N10–12). Both trenches are situated in the main chamber and are separated by a modern visitor path and a large slab of protruding bedrock covered by roof fall (Fig. 1). For the purposes of this study, these two trenches are labeled "Western" and "Eastern" Profile according to their position within the chamber. A partially excavated block of protruding sediment between them is called the "Central Area" (Fig. 1).

A lengthy description of the stratigraphy was published in the Chinese final excavation report (Beijing and Jiangxi 2014), with a translated and modified version presented in the online resources (see Online Resource 1). It is important to note that the 1990s excavators used a separately and independently numbered stratigraphic sequence for each of the profiles, and also used the same numerical labels for either side; thus, with the exception of Layer 4, there is no correlation between layers of the same number from the two systems. In other words, Layer 3A in the WP is not equivalent to Layer 3A (and its subdivisions) in the EP. To avoid confusion, in this report we prepend an area notation to the layers, so that Layer 3A in the WP is "Layer West3A," and in the East, "Layer East3A."

The published descriptions of the stratigraphic layers in the final report for the site (Beijing and Jiangxi 2014) were based on field observations done with the naked eye by the Chinese archeologists (Online Resource 1). Overall, their observations indicate that the sediment in the WP is composed of a silty-clayey matrix with a coarse fraction of sand-sized grains of quartz, schist, and mica (Fig. 4a, c). The lower layers, West4B and West4A, are composed of dark sandy-clay, with limestone and occasional charcoal fragments. Layer West3C2 is a soft but compact sand with large weathered limestone blocks. Layer West3C1B, which contained the earliest pottery, was identified as a reddish brown hard layer with a large quantity of burned clay, charcoal pieces, and weathered breccia. The bottom of this layer exhibits a hard, clay-rich portion that seems unevenly burned. Burned clay fragments are found in

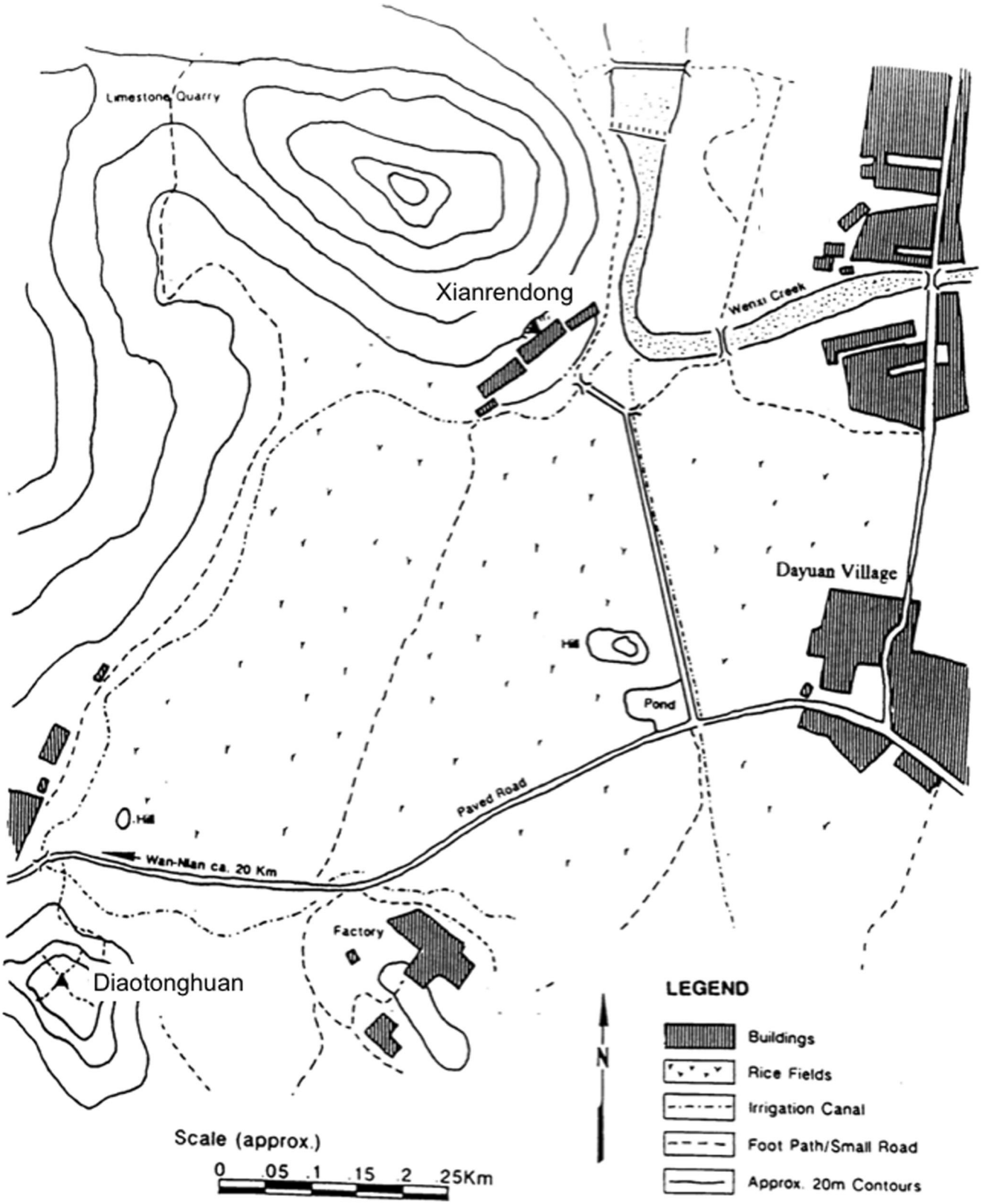

Fig. 2 Topographic map of the vicinity of Xianrendong Cave (after MacNeish and Libby 1995). Wenxi Creek, flowing to the east of the cave, is the only modern watercourse in the immediate surroundings of the site. However, the capacity and course of the creek have been modified by several dams visible on the map. The valley south of the peak is an ancient alluvial valley that is today occupied by rice paddies

Fig. 3 Aerial view of the area around Xianrendong (indicated by the red dot) showing the alluvial valleys that surround the peak that are today cultivated with rice, Wenxi Creek flowing past Dayuan Village, and the dams that have modified its channel (from Google Earth). The star marks the alluvial valley in front of the cave where we hypothesize the watercourse discussed in the text originally flowed

Layers West3C1A, West3B2, and West3B1 above it; these layers also include limestone fragments and some charcoal.

Our observations in the field indicate that whereas the components of the WP seem to be consistent from bottom to top, the sediments in the EP vary vertically (Fig. 4b, d). One key aspect newly noticed in the field in 2009 was the quantity of mica within the different layers, with this observation supported by the micromorphological analysis (see below and Online Resource 2). Following the descriptions in the excavation report, Layer East5A, near the base, is composed of reddish brown sandy-clay with coarse sand and some breccia pieces coated in sandy silt. The layers above, East4B and East4A, are composed of dark sandy-clay with limestone and occasional charcoal. While the early excavators of the site noted that these layers extended to both sides of the cave, we did not find evidence to support this in the re-opened WP. Layer East3B is yellowish brown sandy clay with medium and fine quartz sand and breccia fragments; abundant charcoal pieces are mixed with the upper part of the layer, mostly in the center area. Layer East3A1 is the first one in this profile to be sampled for micromorphology. It is composed of gray silt, with a coarse fraction of sand-sized quartz, feldspar, and small amounts of mica. This layer is sandwiched between bands of coarse gravel ~2.5-cm thick. Layer East2B2 is a reddish-brown sandy silty clay with clay clumps. Calcium carbonate concretions and limestone gravel and breccia appear to be

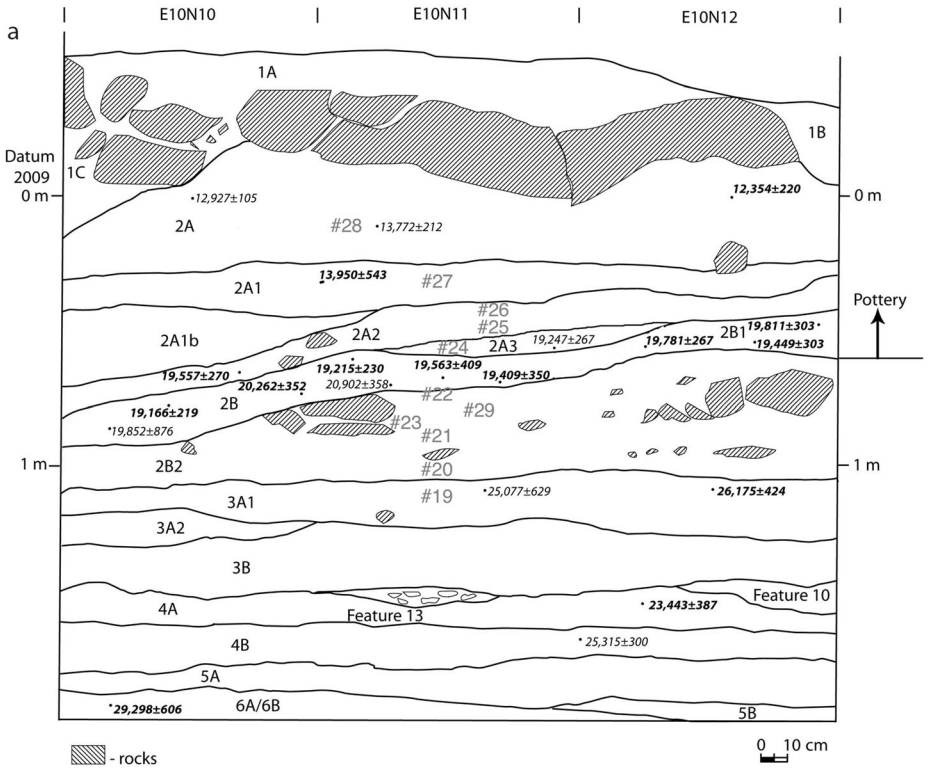
a
E10N10
E10N11
E10N12
Datum
2009
0 m
1 m
1A
1B
1C
2A
2A1
2A1b
2A2
2A3
2B
2B1
2B2
3A1
3A2
3B
4A
4B
5A
5B
6A/6B
Feature 13
Feature 10
Pottery
#19
#20
#21
#22
#23
#24
#25
#26
#27
#28
#29
12,354±220
13,950±543
19,247±267
19,781±267
19,811±303
19,449±303
19,563±409
19,409±350
19,215±230
20,902±358
19,557±270
20,262±352
19,166±219
19,852±876
25,077±629
26,175±424
23,443±387
25,315±300
29,298±606
- rocks
0 10 cm

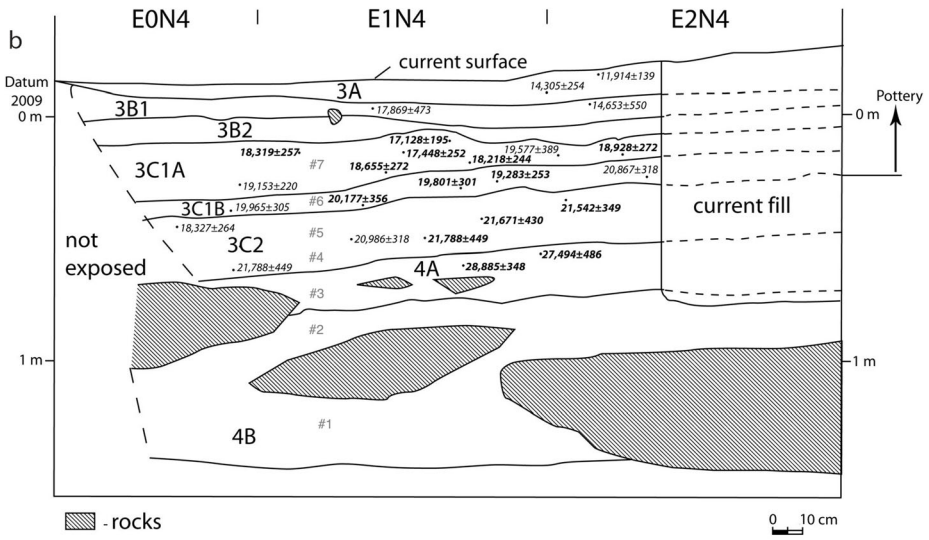
b
E0N4
E1N4
E2N4
Datum
2009
0 m
1 m
current surface
3A
3B1
3B2
3C1A
3C1B
3C2
4A
4B
not
exposed
current fill
Pottery
#1
#2
#3
#4
#5
#6
#7
14,305±254
11,914±139
17,869±473
14,653±550
18,319±257
17,128±195
17,448±252
18,655±272
18,218±244
19,577±389
18,928±272
19,153±220
19,801±301
19,283±253
20,867±318
19,965±305
20,177±356
21,542±349
18,327±264
21,671±430
20,986±318
21,788±449
27,494±486
21,788±449
28,885±348
- rocks
0 10 cm

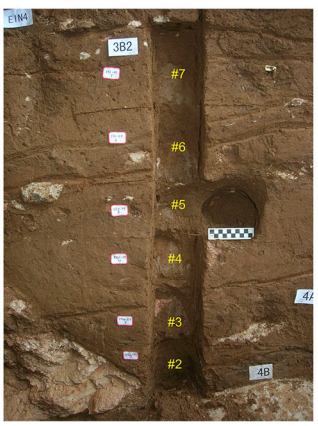
c
E1N4
3B2
#7
#6
#5
#4
#3
#2
4B

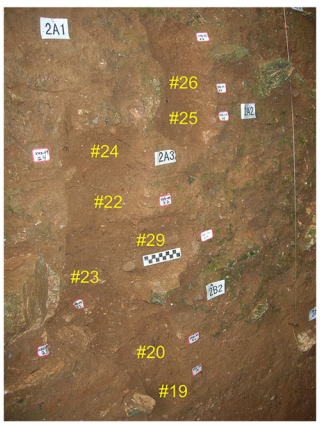
d
2A1
#26
#25
#24
2A3
#22
#29
#23
#20
#19

◀ **Fig. 4** **a** Xianrendong WP with locations of the micromorphology samples indicated. **b** Xianrendong EP with locations of the micromorphology samples indicated (modified from Wu et al. 2012). **c** Photo of the WP with locations where block samples were removed indicated. **d** Photo of the EP with locations where block samples were removed indicated

more abundant in the lower part of the layer. The layer is of uneven thickness, and it thins and disappears toward the south. Layers East2B (which contains the earliest pottery) and East2A3 are compact brown sandy-loams with limestone breccia inclusions and charcoal. Layers East2A2, East2A1, and East2A are dark sandy clay with limestone breccia inclusions. Layer East2A2 is relatively loose, whereas both East2A1 and East2A are compact. Layer East2B is a dark red sandy-silt with loose structure and abundant angular gravelly inclusions. The original excavators note that this earliest-pottery containing layer did not seem to be disturbed. The uppermost Layer, East1A, is light gray silt with cemented shells.

Chronology and dating

There are no dates nor radiocarbon samples from the 1960s excavations due to the chaos of the Cultural Revolution and the closure of many academic institutions during that period. The excavations in the 1990s with better stratigraphic controls yielded a large series of radiocarbon determinations. However, as mentioned above, MacNeish et al. (1998) chose to select those dates that seemed to match dates of early pottery known from Jomon contexts in Japan and they rejected dates that were earlier. They thus selected only seven radiocarbon determinations as acceptable out of 34 samples dated and tried to support this using pollen studies (MacNeish and Libby 1995; MacNeish et al. 1998; MacNeish and Libby 1999). MacNeish and Libby (1999) explain that they rejected the many dates due to what they perceived as inadequate and poor samples, supposed problems with equipment at the Peking University (BA) laboratory not being up to date and reliable, and possible $CaCO_3$ contamination of the ^{14}C samples. It is clear today that these issues are not relevant anymore (Cohen et al. 2017).

The main purpose of the 2009 operation was to clarify the chronology of the layers at Xianrendong, and 45 samples of bone or charcoal fragments each > 1 cm in size were dated (Tables 1 and 2). The bone samples also included faunal remains excavated in the 1990s stored at Peking University in addition to those collected from the re-exposed profiles (Wu et al. 2012). The criterion for only dating samples of size > 1 cm was based on the micromorphological assessment showing samples of this size would not have been moved from original depositional contexts by post-depositional processes. The chronology published by Wu et al. (2012) places the first appearance of pottery at the site at ca. 20,000 cal BP, with the earliest sherds found in Layers West3C1B and Layers East2B and East2B1 (Fig. 4a, b). These results confirm as correct the radiocarbon dates produced in the 1990s that were associated with the earliest pottery but rejected by MacNeish.

The 2009 results also provide many more chronological details for the history of the deposits of the cave. First, they show geogenic sedimentation earlier than 29 ka cal BP (Layers East6B and West4A). The nature of human occupation is also shown to be intermittent, occurring between 25,000 cal BP and 9000 cal BP (Wu et al. 2012). The lack of a radiocarbon record between 17,500 and 14,500 cal BP (Wu et al. 2012) is difficult to interpret, and could be due to either a period of non-deposition or to erosion of the deposits; it is impossible therefore to conclude whether the cave was occupied during this time. The micromorphology, as discussed below, also can clarify the in situ nature and stability of the contexts of the radiocarbon samples, and can aid in further reconstructing the depositional and human behavioral contexts for the pottery and other material culture found here.

Methods

This micromorphological analysis of the sediments of Xianrendong Cave is designed to identify their components and their nature and in turn to reconstruct both the geological and human behavioral contexts of the material culture found in the cave. Twenty-four undisturbed sediment blocks were collected from the EP and WP (Figs. 1 and 4): samples 1 to 7 are from the WP, and samples 19 to 29 are from the EP (Online Resource 2). Samples 9 to 13, determined to be from a backfilled trench, are excluded, and samples 14 to 18, from the upper layers of the central profile, are not studied here, as their stratigraphic placement relative to the other profiles is not clear at present. In both WP and EP, the sediment sample blocks were collected from vertical exposures and include each layer and the boundaries between them (Figs. 1 and 4). After removing the intact blocks, they were wrapped tightly in tissue paper and packaging tape in the field to ensure stability during transport.

At the Micromorphology Laboratory at Boston University, the blocks were oven dried for several days at 60 °C. They were then impregnated with a mixture of 7 parts unpromoted polyester resin and 3 parts styrene catalyzed with methyl-ethyl-ketone-peroxide (MEKP; 8 mL per liter of mixture). Once the resin had gelled, the samples were placed in the oven overnight at 60 °C to complete the process. After impregnation, representative areas were selected for petrographic thin sectioning; in the case of long blocks, two parts were chosen (labeled A, upper; and B, lower). The blocks were trimmed with a rock saw to produce 50 × 75 × 10 mm chips that were sent to Spectrum Petrographics (Vancouver, WA, USA) for processing into thin sections. To facilitate μ-FTIR analysis (see below) the slides were left uncovered.

Table 1 Radiocarbon determinations from Xianrendong WP

Laboratory number	^{14}C Date (Libby half-life)	Calibrated age range year BP 1σ	Material
Layer West2A			
BA09891	10,210 ± 50	11,914 ± 139	Bone
Layer West3A			
BA09894	12,240 ± 55	14,305 ± 254	Bone
Layer West3B1			
BA093181	14,610 ± 290	17,869 ± 473*	Charcoal
Layer West3B2			
UCR3561	12,420 ± 80	14,653 ± 350*	Human bone
Layer West3C1A			
BA09872	14,235 ± 60	17,448 ± 252	Bone
BA09868	14,925 ± 70	18,218 ± 244	Bone
BA09875	13,885 ± 55	17,128 ± 195	Bone
BA09874	15,165 ± 55	18,319 ± 257	Bone
BA00006	15,655 ± 194	18,928 ± 272	Bone
UCR3562	16,010 ± 70	19,153 ± 220*	Human bone
BA95143	16,340 ± 200	19,577 ± 389*	Charcoal
Layer West3C1B			
BA10264	16,165 ± 55	19,283 ± 253	Bone
BA10266	16,485 ± 55	19,801 ± 301	Bone
UCR3439	16,730 ± 120	19,965 ± 305*	Charcoal
BA00007	16,915 ± 186	20,177 ± 356	Bone
AA15005	17,420 ± 130	20,867 ± 318*	Charcoal
UCR3440	18,520 ± 140	22,120 ± 335*	Charcoal
Layer West3C2			
UCR3300	15,180 ± 90	18,327 ± 264*	Human skull
UCR3522	17,580 ± 80	20,986 ± 318*	Charcoal
BA09878	17,915 ± 80	21,542 ± 349	Bone
BA00008	17,983 ± 177	21,671 ± 430	Bone
BA93182	18,110 ± 270	21,788 ± 449*	Charcoal
Layer West4A			
BA00009	22,902 ± 322	27,294 ± 486	Bone
BA09880	24,080 ± 95	28,885 ± 378	Bone

Dates marked with an asterisk are from MacNeish and Libby (1995). Layer West3C1B contained the earliest pottery in this section. Laboratory codes: BA = Peking University Radiocarbon Laboratory; UCR = University of California, Riverside Radiocarbon Laboratory; AA = NSF-Arizona AMS Laboratory, Tucson. Ch indicates a charcoal sample (after Wu et al. 2012). Dates calibrated by CalPal-HULU.2007 version, 1-standard deviation (from Wu et al. 2012)

Table 2 Radiocarbon determinations from Xianrendong EP

Laboratory number	14C Date (Libby half-life)	Calibrated age BP 1δ	Material
Layer East2A			
BA00004	10,456 ± 118	12,354 ± 220	Bone
BA95138	11,840 ± 150	13,772 ± 212*	Charcoal
Layer East2A1			
UC-R3558	11,020 ± 60	12,927 ± 105*	Human bone
BA99038	11,840 ± 380	13,950 ± 543	Bone
Layer East2A2			
BA09899	16,330 ± 65	19,557 ± 270	Bone
Layer East2A3			
BA95139	16,110 ± 140	19,247 ± 267*	Charcoal
Layer East2B1 (earliest pottery)			
BA10263	16,030 ± 55	19,166 ± 219	Bone
BA09912	16,495 ± 60	19,811 ± 303	Bone
Layer East2B (earliest pottery)			
BA09902	16,095 ± 65	19,215 ± 230	Bone
BA10268	16,270 ± 65	19,449 ± 310	Bone
BA00015	16,301 ± 157	19,499 ± 350	Bone
BA99037	16,330 ± 220	19,563 ± 409	Bone
BA09926	16,345 ± 70	19,581 ± 267	Bone
BA95141	16,580 ± 260	19,858 ± 376*	Charcoal
BA10271	17,105 ± 60	20,467 ± 352	Bone
BA95140	17,460 ± 210	20,902 ± 358*	Charcoal
Layer East3A			
BA95142	20,940 ± 440	25,077 ± 629*	Charcoal
BA09921	21,820 ± 85	26,175 ± 424	Bone
Layer East4			
BA00003	19,634 ± 186	23,433 ± 387	Bone
BA95144	21,090 ± 660	25,315 ± 900*	Charcoal
Layer East6B			
BA99039	24,500 ± 370	29,298 ± 606	Bone

Dates marked with an asterisk are from MacNeish and Libby (1995). Layers with the earliest pottery are East2B1 and East2B (after Wu et al. 2012). Laboratory codes: BA = Peking University Radiocarbon Laboratory; UCR = University of California, Riverside Radiocarbon Laboratory. Ch indicates a charcoal sample. Dates marked with an asterisk are cited by MacNeish and Libby (1995). Dates calibrated by CalPal-HULU.2007 version, 1-standard deviation (from Wu et al. 2012)

The petrographic thin sections were scanned on a flat-bed scanner at 2400 dpi with the lid open producing a "dark field" (Goldberg and Aldeias 2018). The thin sections were examined using a microfilm reader, and binocular and petrographic microscopes in plane-polarized light (PPL), cross-polarized light (XPL), and oblique incidence light (OIL) at various scales from × 5 to × 200 (Courty et al. 1989). Descriptive nomenclature follows that of Stoops (2003) and Courty et al. (1989).

In order to identify and quantify the effects of heating, fragments of bone and clay aggregates in the thin sections were analyzed by μ-FTIR (Fourier Transform Infrared Spectroscopy microscope) at the Center for Archeological Science at the University of Tübingen using an Agilent Technologies Cary 600 series FTIR machine equipped with a Cary 610 microscope. The spectra were recorded directly on the thin sections using transmitted and attenuated total reflectance (ATR) mode fitted with a Germanium crystal (see Berna et al. 2007; Berna and Goldberg 2007; Simms et al. 2013).

Transmitted mode was used for the mineralogical analysis of clays recording wavenumbers between 4000 and 2000 cm^{-1}. The Germanium ATR crystal was used for the mineralogical analysis of bone between 2500 and 600 cm^{-1} wavenumbers.

Results

Micromorphological analysis

Microscopic observations of the sample thin sections reveal variations in organization, texture, and fabric of the main constituents of the sediments. The basic components of sand, clay, and mica are generally uniform within each individual profile, although their microstructure, organization, and percentage vary both vertically and horizontally. In the following sections, we highlight the key features of the micromorphological observations. Details are illustrated in Online Resource 2 and in Figs. 5–18. As there are significant differences between the EP and WP, we report on the micromorphological content of each profile separately.

Western profile

Micromorphological analysis (Online Resource 2) shows that the sediments in the WP are overall uniform in composition, texture, and fabric from bottom to top. The sediments can be differentiated into layers based on differences in the relative quantities of each component and the void patterns (see below), with the 1990s field archeologists relying primarily upon visible differences in the quantities of silts and clays to divide the sediments into the different archeological layers that we continue to use in this study. The sediments have a silty-clay matrix with a coarse fraction of sand-sized quartz and mica, along with some sporadic fragments of schist, which when weathered, liberate mica into the matrix. Post-depositional features include redoximorphic features, such as Fe–Mn mottling and nodules formation (Figs. 5 and 6) and secondary carbonate features, secondary $CaCO_3$ cementation, and needle-like $CaCO_3$ coatings and infillings in root passages and fissures (Fig. 6) (see Durand et al. 2010; Lindbo et al. 2010; Vepraskas et al. 1994). Localized clay fissure infillings (Fig. 7) and hydromorphic clay hypocoatings are also frequent and are found in relation to clay depleted groundmass (Fig. 8). These features imply water moving through the sediments.

Subrounded clayey aggregates are also present, but in low numbers (Fig. 9). These aggregates are opaque due to the high Fe–Mn content and when analyzed with μ-FTIR do not show signs of having been heated (see Online Resource 3). We observed only a few isolated fragments of partially phosphatized limestone. These likely originated further back in the cave, but their origin and mode of transport are not clear, and their frequency is so low that we do not discuss them further here. Small fragments of bone and small mammal teeth—which occur in very low abundance—are found in most samples (Fig. 10), with the exception of samples 1A, 2B, and 2A (Layer West4B). Humified plant material is present throughout the profile. The general scarcity of bone, ash, and charcoal in the sediments underlines the general lack of anthropogenic inputs in the deposits of the WP.

Overall, the sediments in the WP are massive, very compact, and with little or no bioturbation (see Online Resource 2) (Fig. 11). Exceptions were noticed in sample 3A (Layer West4A), which has a subangular-blocky structure, and sample 1A (Layer West4B) and possibly sample 6 (Layer West3C1B), which exhibit planar lenticular fissures (Fig. 12) consistent with ice-lensing (Van Vliet-Lanoë et al. 1984; Van Vliet-Lanoë 1987). We also observed clay depletion hypocoatings (Fig. 8) and infillings (Fig. 7): these are formed when percolating water removes clay from the groundmass, redepositing it in the voids. Calcitic coatings and recrystallized calcite (Fig. 6) are also present. Redoximorphic features, such as Fe–Mn depletion hypocoatings, Fe–Mn quasicoatings, and Fe–Mn mottling and nodules (Figs. 5 and 6) are present in every sample. Mottling and staining are for the most part small but very frequent, suggesting short periods of water stagnation. The Fe–Mn redoximorphic features seem to always postdate the calcite (Fig. 6), being superposed on the groundmass and the calcitic features. Water saturation of the sediments in the cave is still occurring today: during our fieldwork in 2009, we observed the bases of both trenches being filled with ~40 cm of standing water due to a rise in the water table following a rainstorm (Fig. 13).

Eastern profile

Micromorphological results show that in contrast to the WP, which mainly features uniform composition and organization, the sediments in the EP vary vertically (Online Resource 2). Throughout the profile, both the fine and the coarse fraction include geogenic as well as anthropogenic materials. The fine fraction is mainly composed of a silty-clayey matrix with abundant ash crystals that have been recrystallized (Fig. 14). The coarse fraction is composed of limestone fragments, quartz sand, schist fragments, and low amounts of mica. As in the WP, some slides have visible fragments of weathered schist, which supplies mica to the matrix. The amount of mica remains uniform across all layers in the WP, whereas in the EP the quantity of mica in different layers fluctuates. In particular, the quantities of mica diminish upwards between samples 19 through 24 (Layers East3A1 and East2B), coinciding with a change of fabric and microstructure in these samples. Samples 19A and 19B (Layer East3A1) are more compact, showing some diffuse bedding, and they contain more mica and no evidence for anthropogenic input (Fig. 15a). Layer East3A1 is similar to the sediments observed in the WP. Changes in

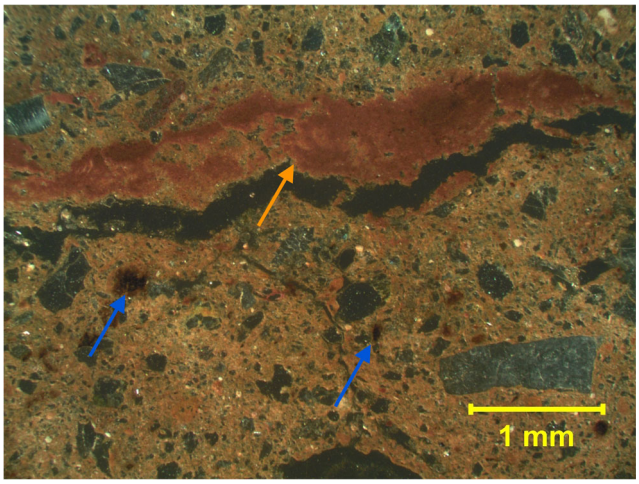

Fig. 5 Fe–Mn oxide hypocoating (orange arrow) and some Fe–Mn mottling (blue arrow) in a sandy-clay matrix in Layer West4A (sample 3A, OIL). Fe–Mn redoximorphic features like these can be found throughout the profile and are evidence for a waterlogged environment

texture, composition, and fabric occur mostly between samples 19 and 20 (Layers East3A1 and East2B2) and between 20 and 24 (Layer East2B) (Fig. 15a–c). Samples 20 to 22 (Layer East2B2) do not show diffuse bedding; instead, they have a complex and open microstructure with no specific arrangement of the components, and are relatively porous expressed by large fissures, chambers, and vesicles (Fig. 15b, c). These samples contain significantly less mica than the sediments in the layer below (East3A1), but contain large bone fragments, ash that has been recrystallized (Fig. 14), and occasional charcoal. The samples in the upper layers, 24 (Layer East2B) to 28 (Layer East2A), are more compact with lower porosity composed of fissures, chambers, and vesicles (Fig. 15c). The components are composed of unoriented silty clay, quartz sand, large limestone fragments, very low to no mica, recrystallized ash, heated bone fragments, and charcoal (Fig. 16).

Unlike the WP, the EP contains clear evidence of human input. Abundant bone was found throughout the profile (Fig. 16), some of which show features consistent with fish bones. Most bone fragments show evidence of having been exposed to heat (Fig. 16a, b) by their darker color. Furthermore, some of the bone fragments exhibit unusual interference colors due to diagenetic processes that are currently being investigated. In addition to bone, other anthropogenic components include fragments of charcoal and ashes (Fig. 16c). Several fragments of freshwater mollusks were observed, but it is not clear whether they are anthropogenic or are of alluvial origin (see below).

Clay aggregates are present throughout the EP and in higher amounts than in the WP. The few clay aggregates found in samples 19 and 20 show indistinct or randomly striated b-fabrics (see Stoops 2003); however, most clay aggregates in samples 21 to 29 above these are isotropic.

Post-depositional processes are more frequent and evident in the EP. Samples throughout the profile also contain Fe–Mn orthic nodules, mottling, and hypocoatings (Fig. 17a, b). These redoximorphic features, which form in waterlogged environments, are consistent with the localized clay coatings and intercalations. Layer East3A1 (samples 19B and 19A) (Fig. 15) is compact with few signs of bioturbation. The sediments in Layer East2B2 (samples 20, 21, 23, 29, and 22B) (Fig. 15) have a subangular to angular structure. However, it is important to note that the space between the peds never exceeds 5 mm in width and that within the peds the matrix is quite compact (Fig. 15). Layer East2B2 is the most affected by bioturbation, while the layers above are quite massive and cemented by secondary calcite probably derived from the dissolution and re-precipitation of ash (Fig. 17c, d), as is suggested by the relicts of ash rhombs in the matrix (Fig. 14). Microcrystalline calcite can be observed in the voids as well as in the matrix (Fig. 17c, d). However, some bioturbation caused by earthworms and land snails is visible in the upper layers where passages are up to 9 mm in diameter.

In sum, the micromorphological results show the following features: The WP has a uniform composition of a silty

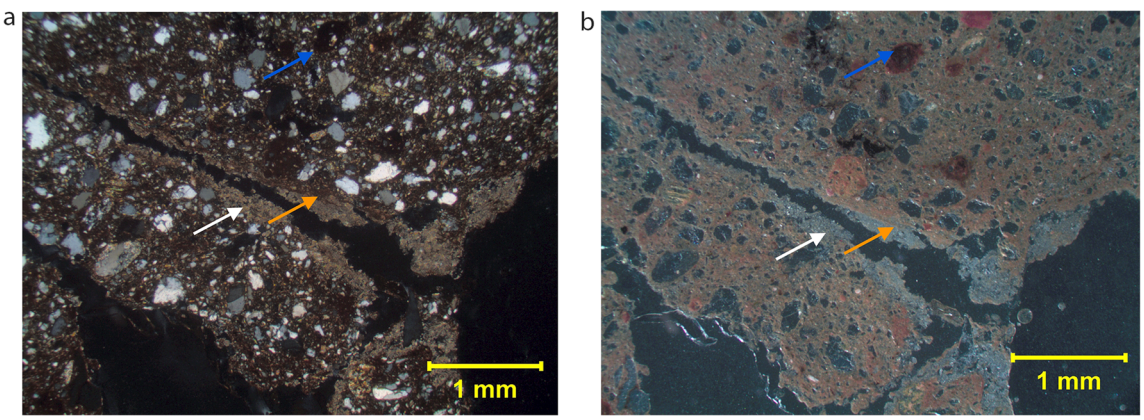

Fig. 6 Secondary micritic coating of a fissure (white arrows) in Layer West3C2, sample 5A. **a** XPL, **b** OIL. Note the Fe–Mn hypocoating (orange arrows) and Fe–Mn mottling and nodule formation (blue arrows). Deposition of secondary calcite is due to evaporation of carbonate-rich waters that percolate through the sediments through voids

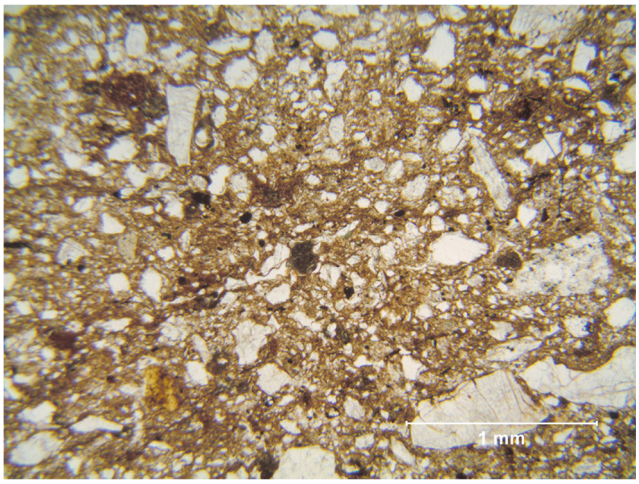

Fig. 7 Horizontal clay intercalation, Layer West3C2 (sample 5B PPL) produced syndepositionally as a slurry with the coarser material

clayey fine fraction with mica- and quartz-rich coarse fraction. Clayey intercalations and infillings and clay-depleted matrix are frequently observed features (Fig. 17e). The sediment is consistently massive and compact with some lenticular fissures in Layer West4B. Similar components and microstructures are visible in the lower strata of the EP, but composition and arrangement of the constituents change in the east starting with Layer East2B2, where amounts of mica diminish though ash, bone, and clay aggregates are abundant. Whereas the lower EP layers are massive and compact, Layer East2B2 has a subangular to angular structure and the layers above are more crumbly. Some bioturbation is visible in Layer East2B2 and above in the form of earthworm passages, but these never exceed 9 mm in diameter. Re-precipitated calcite is present throughout the EP as are Fe–Mn nodules and mottles (for a complete list and description of the layers see Online Resources).

Discussion

The micromorphological analysis of the samples from the EP and WP demonstrates several key dissimilar aspects of the deposits in these two different areas of the cave. These reflect differences in the sources and agents of deposition, as well as post-depositional processes such as bioturbation. Below, we discuss these differences and highlight site formation processes at Xianrendong. The results of our study create a clearer history of the human occupation of the cave through the identification of repeated sedimentary patterns that signal specific human activities there, such as cleaning fire features and dumping fire refuse.

Depositional processes

Micromorphological study along with field observations provide insight into the depositional processes at Xianrendong. It is reasonably clear from the components and their arrangement that the deposits in the western part of the cave are of alluvial origin, while those of the EP are more complex, with both geogenic (alluvial) and anthropogenic deposits. In the WP, repeated low-energy flooding episodes were associated with a watercourse that we hypothesize ran in front of the cave in ancient times, and that sometimes invaded the cave (Fig. 3), resulting in slackwater deposits rich in micaceous clay (see Huang et al. 2012). This inference is supported by the occurrence of clay coatings and clay-depleted coarse fraction quartz domains connected to locally bedded and better sorted coarse fraction, such as in Samples 5A, 5B, and 19B (Figs. 7 and 8) (Brammer 1971). The alluvial origin is also suggested by the presence of rounded clay rip up clasts and disorthic Fe–Mn nodules (Samples 2a, 2b, and 4) (Fig. 9). Although

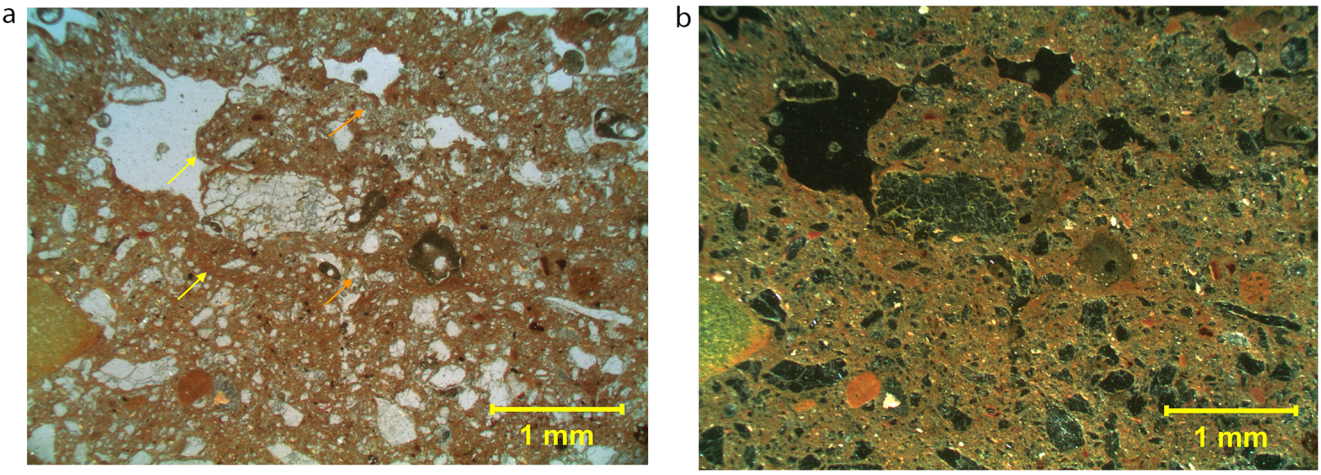

Fig. 8 **a** Clay coatings and intercalations (yellow arrows) in relation to clay depleted groundmass (orange arrows) in Layer West3C2 (sample 5A PPL). Water moving through the sediments will wash out clay and concentrate it elsewhere. **b** Same area shown in OIL to highlight the different colors between the clay coatings and hypocoatings, which appear as bright orange, and the depleted groundmass (sample 5A OIL)

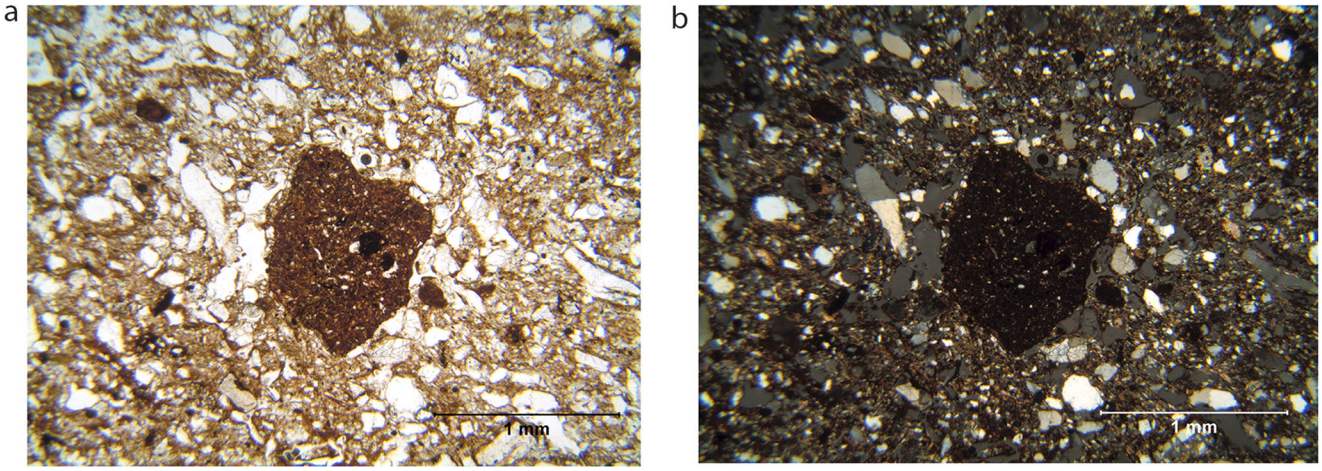

Fig. 9 Subrounded clay aggregate from the WP, Layer West3C2 sample 5B. **a** PPL. **b** XPL. Clay aggregates are abundant in the EP but few are found in the WP. The aggregate shown here, composed of clay and silt size quartz, is dark due to oxidization of Fe–Mn and was not heated, as shown by FTIR, below. This trend suggests that the clay aggregates are geogenic in nature and are not connected to the pottery found in the cave

archeological material was recovered in the WP during excavations, micromorphological observations furnish very limited evidence for anthropogenic inputs. Only a few fragments of bone were observed and most do not show any sign of heating (Fig. 10). The details highlighted here indicate a presence of human input within an overall low energy fluvial regime: however, the nature of the human occupation in the western side of the cave is not clear yet.

The depositional processes of the sediments in the EP are more complex. The lower layers of the EP—Layers East6A/6B to 3A1 (Figs. 15 and 17)—were deposited by water, likely by the same alluvial processes observed in the West. This is indicated by the radiocarbon chronology, the consistent presence of compact silty clay layers with mica and schist observed in the field, and the clay intercalations and clay-depleted domains, compact matrix, and mica observed in thin section (Figs. 15 and 17). Thus, just as in the WP of the cave, the compact micaceous sandy clays in the EP were deposited by low energy floods that appear to have invaded the entire cave vestibule (Fig. 4b). Layer East3A1, the lowest layer for which we have micromorphological samples in this area, contains clear evidence for ephemeral anthropogenic occupation (e.g., ash clumps and micro-charcoal) interbedded with geogenic alluvium. The mixed arrangement of the anthropogenic sediments (bones, ash, and charcoal) point to an original source of a combustion area, but their chaotic arrangement here suggests that this is reworked hearth refuse that was dumped on this side of the cave (Samples 23, 29a, 29b; Online Resource 2). Layer East2B2—composed of sandy clay with visibly less mica than the layers below—is the lowermost deposit to contain consistent anthropogenic inputs, with abundant burned bone, ash, charcoal, and heated clay. We found no evidence of occupational floors or surfaces, again suggesting that Layers East2B, 2A2, and 2A1 represent dumped material (see Macphail and Goldberg 2010; Schiegl et al. 2003). Based on the form of the cave and overall context, it is likely that the

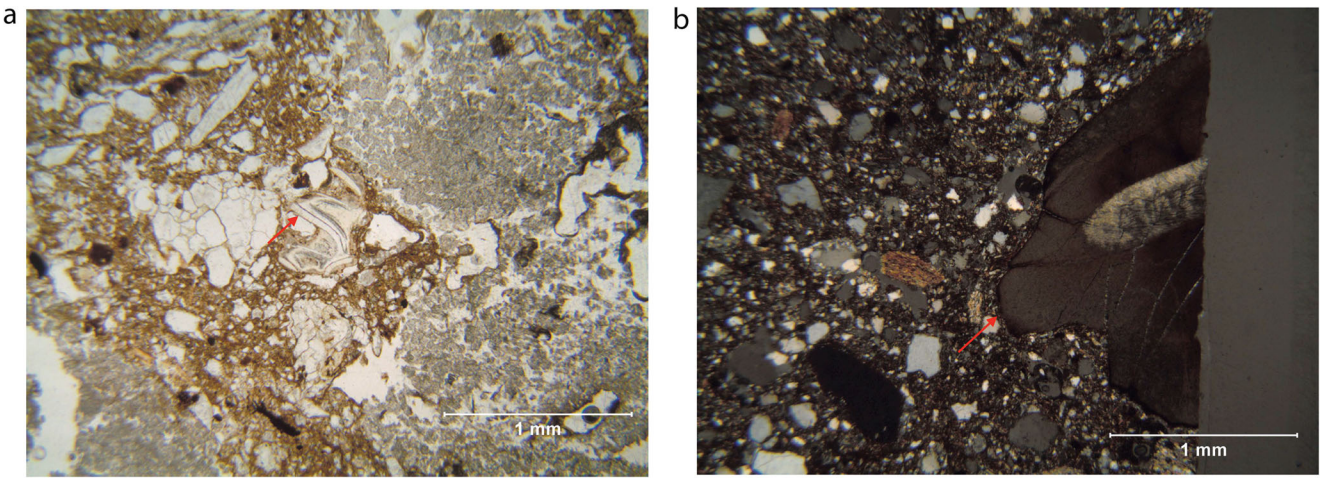

Fig. 10 Unheated tooth and bone matter, Layer West3C2. **a** Fragment of a small mammal tooth likely part of the natural cave components (sample 5B, PPL). **b** XPL photomicrograph of bone fragment (sample 5B, XPL)

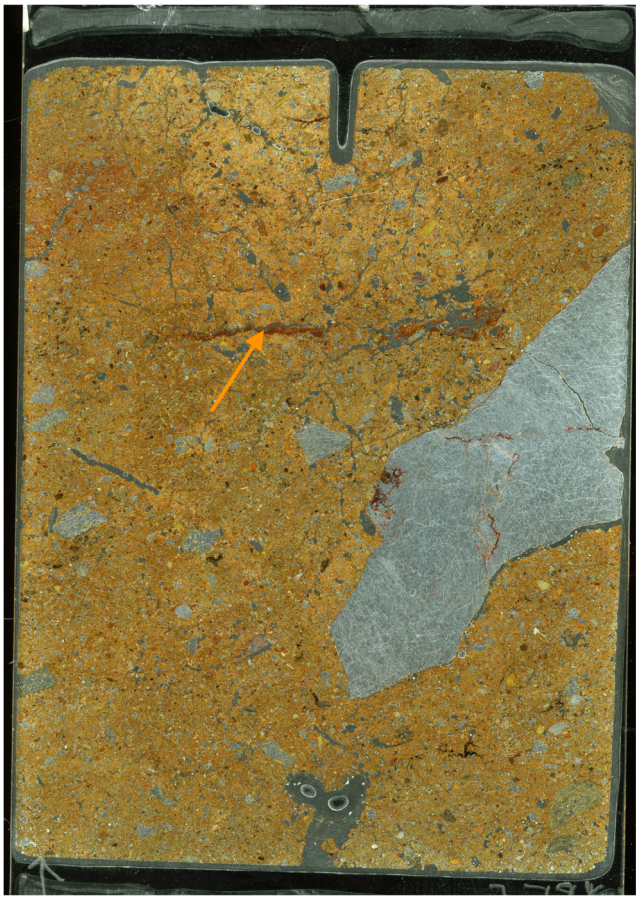

Fig. 11 Scan of sample 3A showing compact and massive microstructure in Layer West4A. Notice the Fe–Mn hypocoating (orange arrow), which is evidence of periodic water saturation (see also Fig. 5)

source of these combusted materials was not at this location nor inside the cave itself, but rather originated outside the strict confines of the cave (see below for a more comprehensive discussion on the chronology of the strata).

Bioturbation and diagenesis

Identification and interpretation at Xianrendong of post-depositional processes in general and bioturbation in particular are critical to a holistic understanding of the archeological and geological record. As shown above, there are only local, small bioturbation features in both profiles. This observation strongly supports the chronology proposed by Wu et al. (2012) for the ca. 20,000 cal BP appearance of pottery at Xianrendong by minimizing the effect of any movement of centimeter-sized objects such as bone that were used in dating. The WP is composed of consistently massive and compact sediments with little porosity and an absence of pedality and bioturbation. Together, they all signal that the artifacts, bones, and charcoal found here were not displaced post-depositionally.

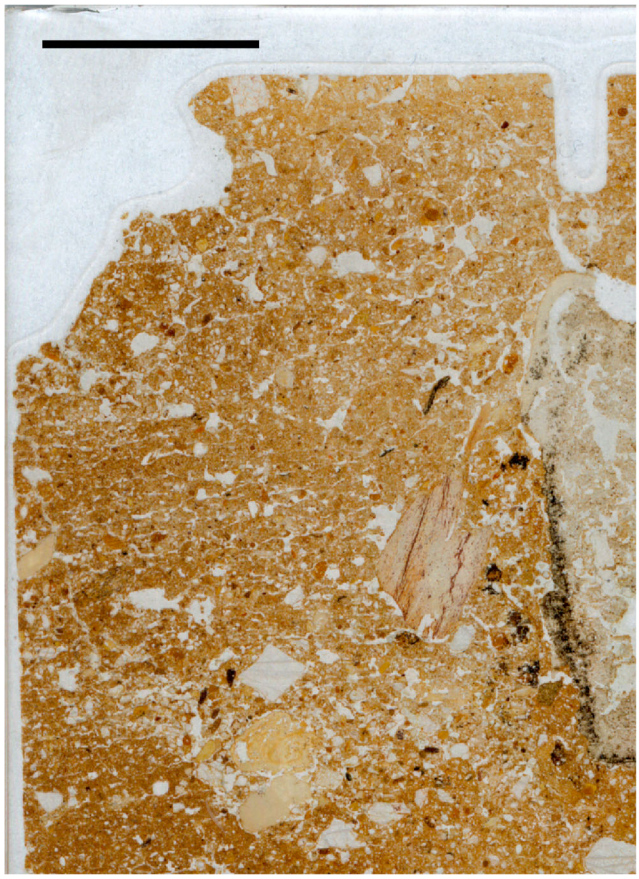

Fig. 12 Scan of upper portion of sample 1A (Layer West4B) at the base of the profile. The top part has a lenticular microstructure. These features are consistent with frost action and suggest that these lowermost deposits' sediments underwent some freeze–thaw. The rarity of these features in the sediments at Xianrendong overall suggests that freezing temperatures were an exceptional occurrence here

Some features, however, can be used as climatic signals. In the lowest sample (Layer West4A), lenticular fissures were observed and are possibly related to occasional freezing and thawing (see Van Vliet-Lanoë et al. 1984; Van Vliet-Lanoë 1987). In addition, Fe–Mn crusts, staining, and orthic nodules are found throughout the profile and suggest periods of stagnant water in the cave throughout its history (see Figs. 5, 6, 13, 14, and 17a, b). Such chemical features supported formation of syndepositional intercalations and some clay coatings: these are linked to periodic flooding (see Brammer 1971). However, we note that in Layer West3C2, for example (Fig. 6), Fe–Mn precipitation can locally postdate the formation of clay coatings. The cave was not water saturated for long periods of time since the Fe–Mn features are not well developed. Instead, we should imagine the occurrence of both dry and wet periods during the accumulation of the WP.

The EP, on the other hand, contains more evidence for bioturbation and diagenesis. Bioturbation, although not prevalent, is present in the form of insect or earthworm passage features with a maximum diameter of 9 mm. It is

Fig. 13 Photo of trench of WP filled with groundwater that had risen after a rainstorm during the 2009 season. Most of the post-depositional features found in the WP are associated with periods of stagnant water like the one shown here

important to note that these millimeter-sized features are not pervasive enough to result in large-scale mixing of sediments from different layers or in movements of objects such as bones of the size used in dating. As mentioned above, the samples from Layer East2A2 have a subangular to crumbly structure. As was the case for the WP, the EP shows evidence of post-depositional water saturation as well as dry periods. In fact, Fe–Mn orthic nodules and staining occur throughout the profile having been produced by saturation from rises in the water table.

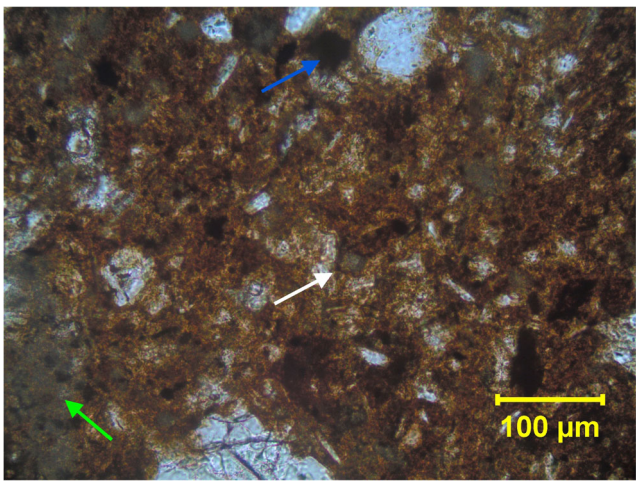

Fig. 14 Silty clay matrix with ash rhombs that have been recrystallized (white arrows) and some Fe–Mn staining (blue arrows) in Layer East2A3 (sample 22B). The middle and upper layers of the EP contain abundant bone, charcoal, and ash. Although the ash is mostly recrystallized (green arrow), often resulting in micritic cementation of the matrix, pseudomorphs of ash rhombs are still visible at higher magnification (white arrows)

The EP is strongly cemented by calcium carbonate. The process of dissolution and crystallization of calcite in caves is a complex one requiring specific conditions and a delicate balance between water precipitation and evaporation, and amounts of CO_2 (see Holland et al. 1964; White 2007). The cementation at Xianrendong is probably the result of a fluctuation between wet and dry periods, with CO_2-rich water dissolving ashes from layers that are ash rich, and the drying process resulting in the precipitation of dissolved carbonates.

Lenticular microstructures, produced by occasional low temperatures that caused the presence of localized ice in the sediments, can be observed in the top portion of sample 20 and possibly 29A (both from Layer East2B2). No other evidence for low temperatures was found in the EP. However, at the Hongguang sand dune in Pengze, ca. 180 km north of Xianrendong cave, interbedded layers of eolian sand beds and thin paleosols formed between 26,000 and 20,000 BP were identified, indicating localized fluctuations, between humid-wet and cold-dry environment (Liu et al. 1997). Occasional freezing temperatures during the deposition of Layer East2B2 are therefore not to be excluded at Xianrendong.

Our field observations also reveal a clear erosional gap expressed in a truncation at the western end of Layers East2B2, 2B, and 2A2. It is difficult at the moment to infer the mode of erosion of these layers. However, particularly with the radiocarbon chronology, we can assert that the timing of erosion must have been either before or contemporaneous with the deposition of Layers West3C2, 3C1B, and 3C1A in the WP (Fig. 4; Tables 1 and 2).

Furthermore, our analysis of the post-depositional processes visible in both the Western and the EPs of Xianrendong clearly shows that any archeological materials greater than

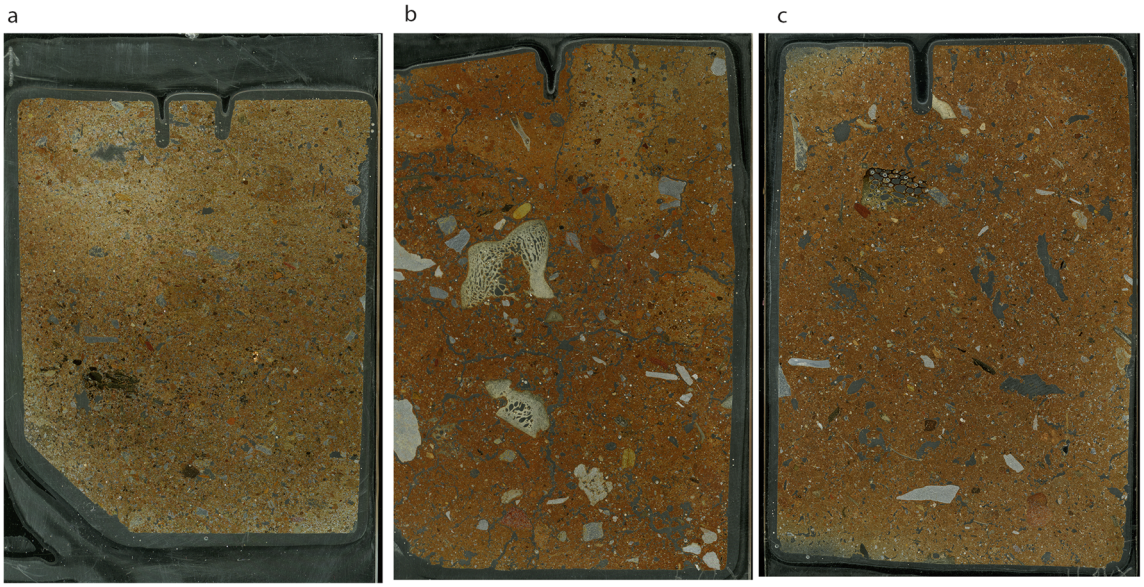

Fig. 15 Macroscans of samples representative of the changes in the overall texture, composition, and fabric of the different layers from the EP. **a** Sample 19B from Layer East3A1, showing a compact microstructure with diffused bedding. **b** Sample 20 from Layer East2B2, showing bones and a complex microstructure with some angular to subangular peds, localized crumbly, compact, and vughy microstructure. Layer East2B2 contains some roof fall, which may have altered the microstructure. **c** Sample 24 from Layer East2B is more compact. Here, the components are not arranged in any specific way

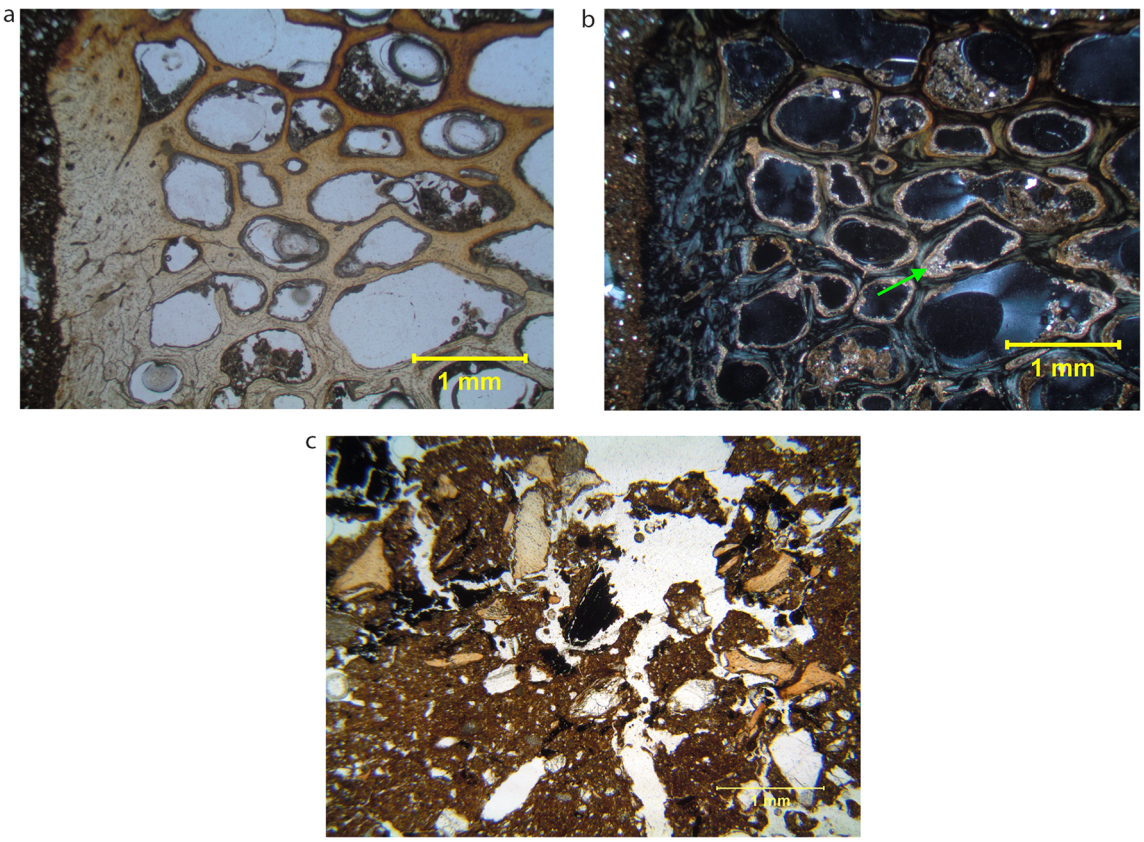

Fig. 16 Bone fragments in Layer East2A3 and East2B2 with evidence of heating (samples 24 and 29). Most bone fragments in layers 2B2 and above show signs of having been heated. **a** Bone from Layer East2A3 (sample 24). The light to dark brown color in the PPL photomicrograph suggests that this fragment was heated. **b** XPL image of the same fragments also shows features connected to heating such as high birefringence of the bone and some micritic calcite in the pores (green arrow). **c** Fragmented bone and charcoal in Layer East2B2 (sample 29A). While the field profile exhibited large pieces of bone, fragmented bone in the sediments shown here is consistent with trampling

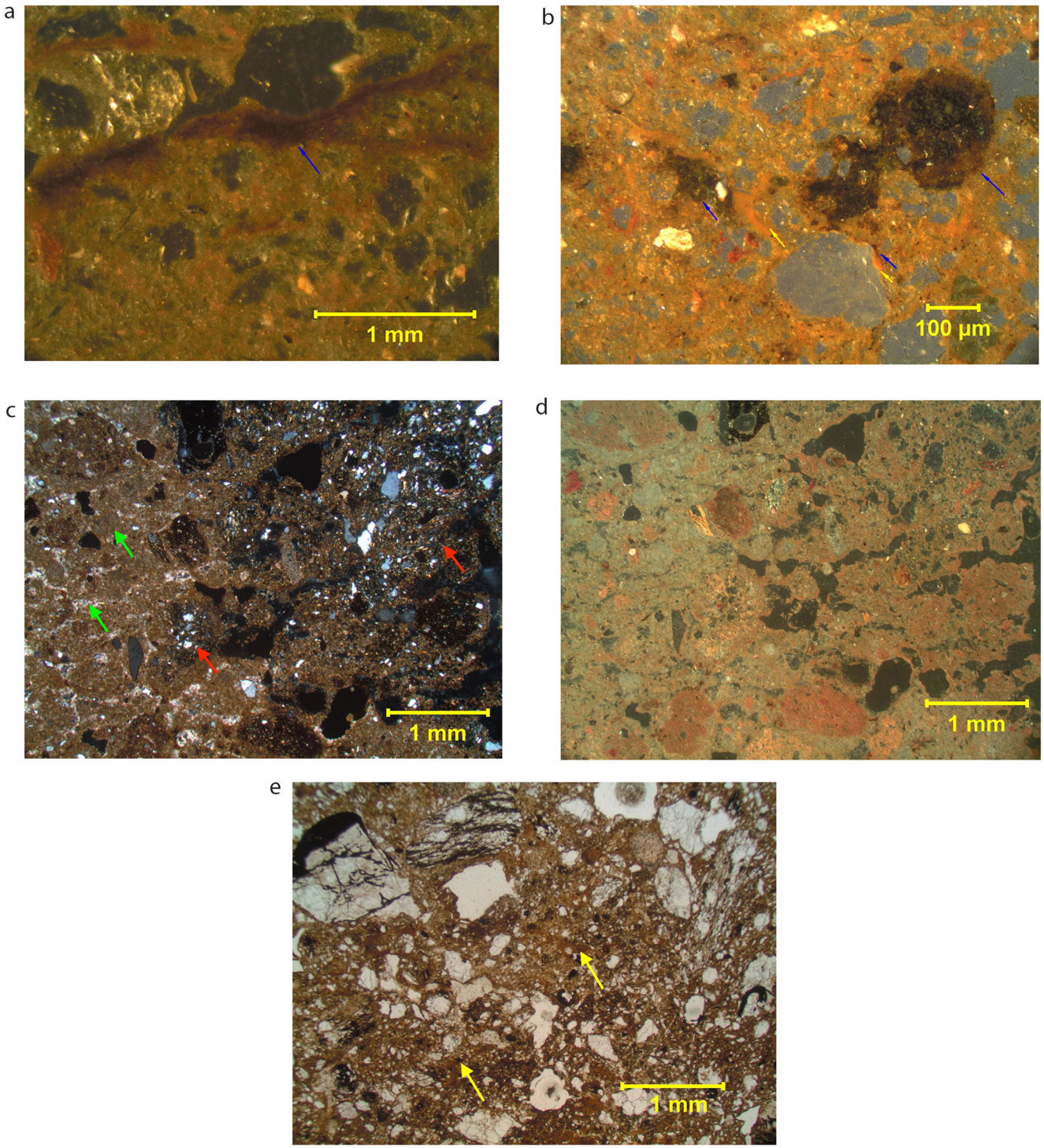

Fig. 17 Examples of some of the post-depositional features observed in the EP. **a** OIL photomicrographs of Fe–Mn vein like precipitation (blue arrows) in Layer East3A1 (sample 19B). Redoximorphic features appear in sediments after 2 to 3 days of water saturation (see text for discussion), and their presence here suggests that the sediments were waterlogged for short periods of time. **b** OIL photomicrograph of Fe–Mn mottling and nodules (blue arrows) and clay coatings and infillings (yellow arrows) in Layer East3A1 (sample 19B). Clay can be transported and redeposited by water percolating through the sediments under conditions such as slack water or dripping water. The Fe–Mn hypocoatings and nodules are superposed on the clay coatings, indicating that they post-date the formation of the clay coatings. **c** $CaCO_3$ depletion (red arrows), infillings of fissures with recrystallized $CaCO_3$, and cementation of matrix with micritic carbonate (green arrows) in Layer East2B2 (sample 20). **d** Same area, shown in OIL to highlight the presence of faint Fe quasicoatings in the calcitic portion. Recrystallization of calcite takes place under wetter conditions. **e** Clay intercalations (yellow arrows) in Layer East3A1 (sample 19B), which are thought to form in waterlogged environments (Stoops et al. 2010) as supported by the presence here of Fr–Mn mottling

1 cm in size deposited in the sediments in both profiles accumulated with the surrounding sedimentary matrix and did not undergo significant post-depositional movement. The bioturbation that we observe, which is mainly due to disturbance by earthworms and insects, would not have been able to dislocate materials of this size. This strongly supports the contextual integrity of the samples used for radiocarbon dating by Wu et al. (2012). Our results can therefore offer confirmation of the security of the dating of Xianrendong and in particular the dating of the lowest pottery-containing layers from each profile to ca. 20,000 cal BP, making the sherds found the earliest examples of pottery vessels yet recovered.

Chronology of sedimentation and human use of the cave

A time–depth plot (Fig. 18a, b) reveals changes in the rate of sedimentation, with periods of non-deposition or erosion and periods of more rapid and conspicuous sediment input. Cross-referencing the data from the WP and the EP, we can reconstruct the overall sedimentological history of the cave and identify a few inconsistencies in the dating.

As previously stated, the WP is composed entirely of alluvial slackwater deposits. The radiocarbon dates point to alluvial sedimentation between ~29,000 and 27,000 cal BP. Moreover, the scatterplot (Fig. 18a) highlights a hiatus in accumulation in the WP between ~27,000 and 21,000 cal BP, thus suggesting either a lack of flooding and/or period(s) of erosion. This hiatus in sedimentation could be due to a shift in the course of or to the disappearance of the watercourse that previously flooded the cave depositing slackwater sediments. Sedimentation starts again between ~21,000 and 18,000 cal BP and continues until ~11,000 cal BP (Layers West3C2 to 3A). The micromorphology confirms the reappearance of alluvial deposition within the upper layers of the WP (Layers West3C2 and above). The cycles of the disappearance and reappearance of water courses near the cave could be connected to localized climatic shifts that were also observed at the Hongguang sand dunes between 26,000 and 20,000 BP (Liu et al. 1997) (see above) or could simply represent lateral mobility of the stream channel. To better understand the local paleoclimate and water channel cycles, a more in-depth study of the landscape around the cave is necessary with particular focus on the alluvial valley in front of the cave.

In the EP, the micromorphological data for Layers East6A to 3A1, deposited between ~29,000–26,000 cal BP, show regular sedimentation that is tied to alluvial input. The layers deposited after ~26,000 cal BP (from Layer East3A1 upward) are anthropogenic, in contrast to the WP. Thus, for ~5000 years, until ca. 21,000 cal BP, sedimentation in the cave appears to occur only in the EP, in response to regular human contributions. At 21,000 cal BP, alluvial inputs reappear and seem to continue until ca. 11,000 cal BP. This reappearance of the alluvium at 21,000 cal BP in the WP and the deposition of the alluvial Layers West3C2 and 3C1B could be connected to the erosional surfaces and truncations noted in Layers East2B2, 2B, and 2A2. Moreover, the consistent dates of these strata across both profiles point to contemporaneous deposition for these alluvial layers in the west and anthropogenic layers in the east. We propose that between ca. 21,000 and 18,000 cal BP, the western portion of the cave was periodically inundated by slackwater. Although there is no micromorphological evidence of human occupation of this part of the cave, stone tools and pottery fragments were recovered here, denoting a possible human presence. However, the nature of the human occupation is still obscure in the west. The sediments in the eastern part do not show traces of alluvial input. We also hypothesize that sediments in the east remained untouched by water entering the western side of the cave either because the deposits were already above the water level or because of other physical barriers not visible today. Only the southern and western edges of the eastern strata seem to have been impacted by flooding, which caused some erosion and truncation (Layers East2B2, 2B, and 2A2).

While the dates of the pottery at Xianrendong are generally accepted, Kuzmin (2013, 2015) disputes the accuracy of the ~20,000 cal BP date for the earliest pottery. Although we do not discuss this issue here (see Cohen et al. 2017), it is important to mention that our reconstruction signals that one date from Layer East3A1 (26,175 cal BP [BA09921]) is a likely outlier (see Online Resource 4). Whereas we do not have a definitive explanation for its greater age than other samples in this layer, we may hypothesize that this could be related to possible human occupation on older alluvial sediments that existed outside the cave. In other words, it is possible that this radiocarbon sample was originally present in older sediments outside the cave and transported inside by humans along with other refuse materials that were being dumped in the interior portion of the cave at the time of deposition of Layer East3A1. This radiocarbon date would therefore point to earlier human activity outside the cave and not the date of the later discard activity that coincided with the true date of the deposition of the layer inside the cave. Our reconstruction shows that the rest of the dates published by Wu et al. (2012) are in sequence and consistent with the intact stratigraphic order. These data, including the evidence for the absence of significant bioturbation, confirms the legitimacy of the ~20,000 cal BP date for the earliest pottery in the cave.

a

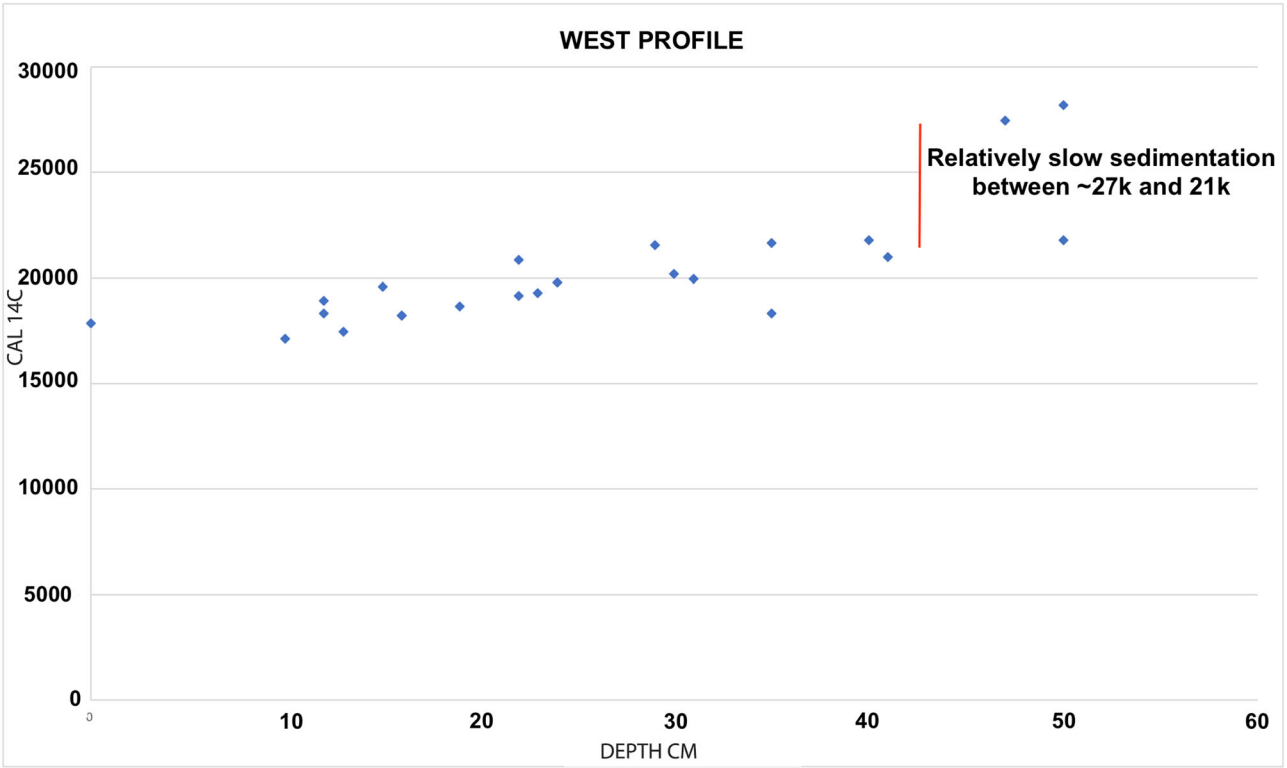
WEST PROFILE
30000
25000
20000
15000
10000
5000
0
CAL 14C
10
20
30
40
50
60
DEPTH CM
Relatively slow sedimentation
between ~27k and 21k

b

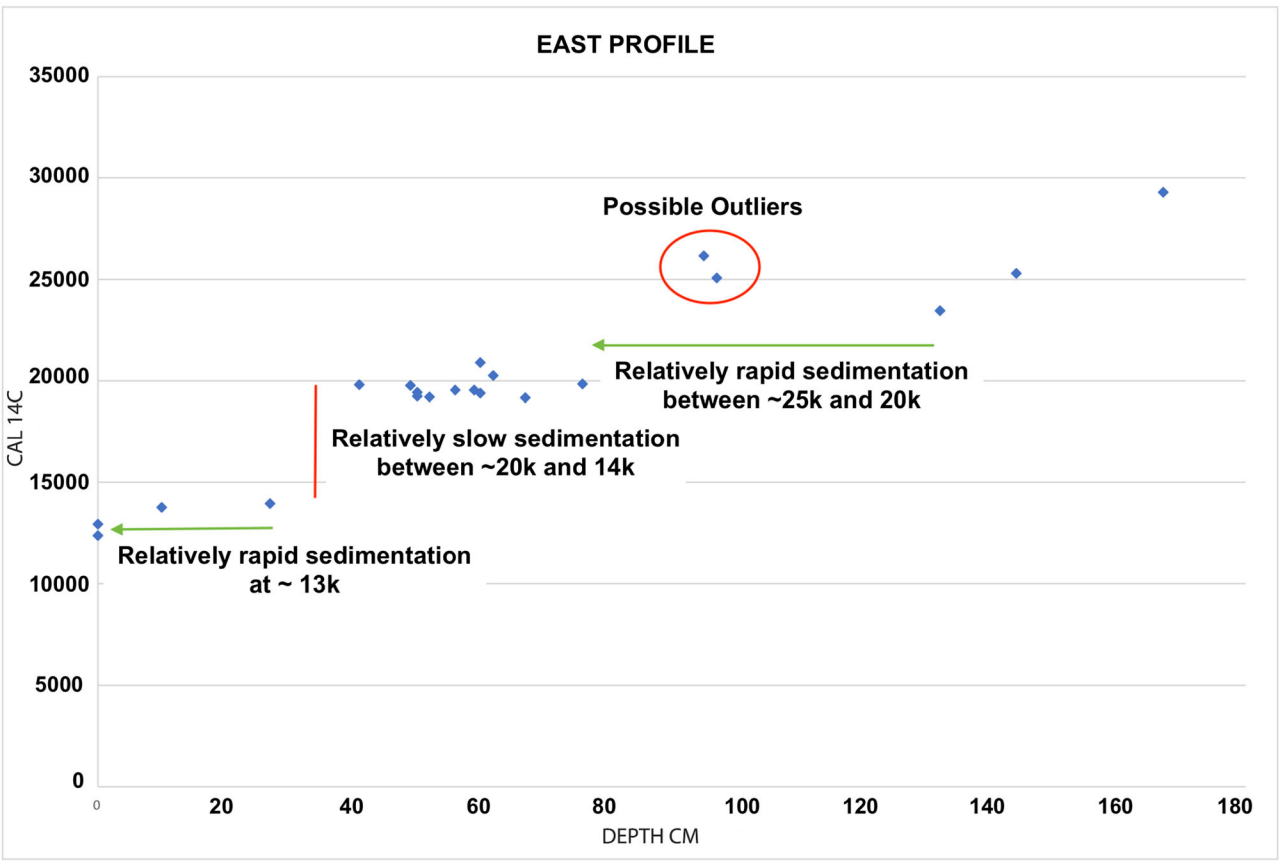
EAST PROFILE
35000
30000
25000
20000
15000
10000
5000
0
CAL 14C
20
40
60
80
100
120
140
160
180
DEPTH CM
Possible Outliers
Relatively rapid sedimentation
between ~25k and 20k
Relatively slow sedimentation
between ~20k and 14k
Relatively rapid sedimentation
at ~ 13k

◀ **Fig. 18** Time–depth plots illustrating depositional rates. **a** The WP shows a depositional hiatus between ~27,000 and 21,000 cal BP, followed by periods of regular input of alluvium. **b** The EP, in contrast, shows moments of relatively rapid sedimentation. Between ~25,000 and 20,000 cal BP, we see the appearance of anthropogenic sediments in the east along with some roof fall that increase the volume of the sediments. Relatively slow deposition in the west between ~20,000 and 14,000 cal BP is coeval with the reappearance of alluvial sedimentation in the east

Human occupation of the cave and use of space

The reconstruction of the site formation processes and the chronology of the sedimentation of Xianrendong provide greater insight into the occupational history of the cave. First, the lack of anthropogenic deposits indicates that human use of the cave prior to 27,000 cal BP is very ephemeral. Although we cannot confirm that humans visited the cave seasonally, occupation of the cave had to take into account the floodwaters that often invaded it. With the interruption of flooding events at 27,000 cal BP, likely related to movement of the river away from the cave, human occupation of the Xianrendong site becomes more conspicuous.

Second, although previously not realized, our data suggest that humans used the space in the eastern part of the cave as a dump where refuse composed of cleaned hearth features and other archeological material accumulated (Samples 22b, 23, 29a, 29b; Online Resource 2). Third, as primary human activities appear to be quite limited inside the cave proper, and because no intact living floor has been identified inside the cave vestibule, it is likely that the main human occupation at the site occurred in an unexcavated area outside of the cave, beyond the current drip line at the entrance. If this is the case, then old alluvial sediments from this area could have occasionally gotten mixed with the anthropogenic trash dumped in the cave. Unfortunately, the area outside the cave was never excavated or tested, as small buildings were present outside the cave entrance from the original excavations in the 1960s through 1990s. It is not clear if these buildings may have disturbed prehistoric contexts. The buildings were removed in recent years in order to establish a site park, visitor path, and railing close to the cave, but excavations outside the cave were never carried out. Our hypothesis for the main location of human activity at the site being outside the cave should be tested in the future.

Conclusions

The micromorphological study of the sediments of Xianrendong cave reported here demonstrates the potential of this approach to reveal the nature of geogenic processes and human activities at the cave: through these, we gain deeper understanding of the human behavioral patterns that led to the deposition of cultural remains in the cave. In light of the evidence for flooding and dumping presented here, previous assumptions concerning human habitation within the cave vestibule need to be reconsidered. While it had long been assumed that people were living inside the cave, our analysis shows no presence of occupational surfaces. These locations only contain refuse that was dumped in the cave but reveal no evidence for the primary activities that created such waste products. The micromorphological analyses coupled with radiocarbon dates reveal the increasing presence of human activity in the cave coinciding with the still cold period just after LGM (~20,000 cal BP). This is the period when the earliest pottery was produced.

Furthermore, this study shows the potential of micromorphology to resolve debated issues concerning the contextual integrity of objects within cultural deposits, especially bones and charcoal that are used as dating samples. Our results lend further support to the validity of the dating of Xianrendong early pottery (Wu et al. 2012; Cohen et al. 2017), as we show that bioturbation at any given time at Xianrendong is very weak. This supports the inference that the radiocarbon-dated materials are contemporary with the stratum of their original deposition and were not moved post-depositionally.

Xianrendong and other caves in South China, such as Yuchanyan in Hunan (Boaretto et al. 2009), show hunter-gatherers producing pottery from 20,000 cal BP onward, some 10,000 years before the first sedentary settlements appear along with the onset of agricultural activities. The specific roles of the caves within hunter-gatherer societies from the LGM through the Terminal Pleistocene, however, remain poorly understood. The micromorphological study here is a first step in gaining such understanding. At Xianrendong, further investigation is needed to support our hypothesis that human activities centered outside the entrance of the cave while within the cave vestibule itself, human behaviors are primarily associated with dumping and not directly with domestic activities such living areas, food preparation and cooking, bone and stone tool and pottery manufacture, or other daily-life activities.

To fully understand human behavior in South China at the time when Upper Paleolithic hunter-gatherers first invented pottery, it is necessary to apply geoarchaeological techniques consistently across the complete set of sites. This must be done in combination with other scientific methods of investigation, as questions of site function, formation processes, and dating remain poorly understood. Such studies should provide better insights into hunter-gatherer adaptations and

activities—including subsistence and ritual behaviors—and in particular into the reasons for the invention of pottery in the context of foraging economies.

Acknowledgments Funding for this project was provided through grants from the National Science Foundation (USA) (no. 0917739 and no. 0551927) and the American School for Prehistoric Research (Peabody Museum, Harvard University). Logistical support was provided by the Jiangxi Provincial Government, Wannian County Government, and Jiangxi Provincial Museum, and we extend our gratitude for their gracious and enthusiastic help.

References

Beijing and Jiangxi (2014) School of Archaeology and Museology Peking University, Jiangxi Province Institute of Cultural Relics and Archaeology (eds). Xianrendong and Diaotonghuang. Cultural Relics Press, Beijing (in Chinese)

Berna F, Goldberg P (2007) Assessing Paleolithic pyrotechnology and associated hominin behavior in Israel. Isr J Earth Sci 56:107–121

Berna F, Behar A, Shahack-Gross R, Berg J, Boaretto E, Gilboa A, Sharon I, Shalev S, Shilstein S, Yahalom-Mack N, Zorn JR, Weiner S (2007) Sediments exposed to high temperatures: reconstructing pyrotechnological processes in late bronze and Iron Age strata at Tel Dor (Israel). J Archaeol Sci 34:358–373

Boaretto E, Wu X, Yuan J, Bar-Yosef O, Chu V, Pan Y, Liu K, Cohen D, Jiao T, Li S, Gu H, Goldberg P, Weiner S (2009) Radiocarbon dating of charcoal and bone collagen associated with early pottery at Yuchanyan cave, Hunan Province, China. Proc Natl Acad Sci U S A 106(24):9595–9600

Brammer H (1971) Coatings in seasonally flooded soils. Geoderma 6:5–16

Cohen DJ (2013) The advent and spread of early pottery in East Asia: new dates and new considerations for the world's earliest ceramic vessels. J Austronesian Stud 4:55–92

Cohen DJ, Bar-Yosef O, Wu X, Patania I, Goldberg P (2017) The emergence of pottery in China: recent dating of two early pottery cave sites in South China. Quat Int 441(Part B):36–48

Courty MA, Goldberg P, Macphail R (1989) Soils and micromorphology in archaeology. In: Cambridge manuals in archaeology. Cambridge University Press, Cambridge

Day MJ, Tang T (2004) Tower karst. Encycl Caves Karst Sci:734–736

Durand N, Monger CH, Canti MG (2010) Calcium carbonate features. In: Stoops G, Marcellino V, Mees F (eds) Interpretation of micromorphological features of soils and regoliths. Elsevier, Amsterdam, pp 149–194

Ford DC, Williams PW (1989) Karst geomorphology and hydrology. Unwin Hyman, London

Goldberg P, Aldeias V (2018) Why does (archaeological) micromorphology have such little traction in (geo) archaeology? Archaeol Anthropol Sci 10:269–278

Holland HD, Kirsipu TV, Huebner JS, Oxburgh UM (1964) On some aspects of the chemical evolution of cave waters. J Geol 72:36–67

Huang CC, Pang J, Zha X, Zhou Y, Su H, Zhang Y, Wang H, Gu H (2012) Holocene palaeoflood events recorded by slackwater deposits along the lower Jinghe River valley, middle Yellow River basin, China. J Quat Sci 27:485–493

Huang W, Deng CB, Day MJ (2013) Differentiating tower karst (fenglin) and cockpit karst (fengcong) using DEM contour, slope, and centroid. Environ Earth Sci 72:407–416

Hughes PD, Gibbard PL (2015) A stratigraphical basis for the last glacial maximum (LGM). Quat Int 383:174–185

Hughes PD, Gibbard PL, Ehlers J (2013) Timing of glaciation during the last glacial cycle: evaluating the concept of a global "Last Glacial Maximum" (LGM). Earth Sci Rev 125:171–198

Jiangxi Provincial Committee on Cultural Relics Management (1963) Report on the test excavation of Xianrendong cave, Dayuan, Wannian, Jiangxi. Kaogu xuebao 1963(1):1–16 (in Chinese)

Jiangxi Provincial Museum (1976) Second report on the excavation of Xianrendong cave, Dayuan, Wannian, Jiangxi. Wenwu 1976(12): 23–35 (in Chinese)

Kuzmin YV (2013) Origin of Old World pottery as viewed from the early 2010s: when, where and why? World Archaeol 45:539–556

Kuzmin YV (2015) The origins of pottery in East Asia: updated analysis (the 2015 state-of-the-art). Doc PraehistI XLI:1–12

Lindbo DL, Stolt MH, Vepraskas MJ (2010) Redoximorphic features. In: Stoops G, Marcellino V, Mees F (eds) Interpretation of micromorphological features of soils and regoliths. Elsevier B.V., New York, pp 129–147

Liu J, Wu X, Li Z, Zhang M (1997) The last glacial stratigraphic sequence, depositional environment and climatic fluctuations from the Aeolian sand dune in Hongguang, Pengze, Jiangxi (China). Quat Sci Rev 16:535–546

MacNeish RS, Libby JG (1995) Origins of rice agriculture, the preliminary report of the Sino-American Jiangxi (PRC) Origin of Rice Project SAJOR. Andover Foundation, Andover

MacNeish RS (1999). A Paleolithiceneolithic sequence from South China Jiangxi Province, PRC. In: Omoto, K. (Ed.), Interdisciplinary Perspectives on the Origins of the Japanese. International Research Center for Japanese Studies, Kyoto

MacNeish RS, Libby JG (1999) A Paleolithic–Neolithic sequence from South China Jiangxi Province, PRC. In: Omoto K (ed) Interdisciplinary perspectives on the origins of the Japanese. International Research Center for Japanese Studies, Kyoto, pp 233–255

MacNeish RS, Cunnar G, Zhao Z, Libby J (1998) Second annual review of the Sino-American Jiangxi (PRC) Origin of Rice Project SAJOR. Andover Foundation, Andover

Macphail RI, Goldberg P (2010) Archaeological materials. In: Stoops G, Marcellino V, Mees F (eds) Interpretation of micromorphological features of soils and regoliths, pp 597–630

Schiegl S, Goldberg P, Pfretzschner H, Conard NJ (2003) Paleolithic burnt bone horizons from the Swabian Jura: distinguishing between in situ fireplaces and dumping areas. Geoarchaeology 18:541–565

Simms SR, Berna F, Bey GJ (2013) A prehispanic Maya pit oven? Microanalysis of fired clay balls from the Puuc region, Yucatán, Mexico. J Archaeol Sci 40:1144–1157

Stoops G (2003) Guidelines for analysis and description of soil and regolith thin sections. Soil Science Society of America Inc., Madison

Stoops G, Marcellino V, Mees F (eds) (2010) Interpretation of micromorphological features and regoliths. Elsevier B.V., Amsterdam

Van Vliet-Lanoë B (1987) Dynamique périglaciaire actuelle et passée : apport de l'étude micromorphologique et de l'expérimentation. Buletin de 'AFEQ 24:113–132

Van Vliet-Lanoë B, Cotard J, Pissart A (1984) Structures caused by repeated freezing and thawing in various loamy sediments: a comparison of active, fossil and experimental data. Earth Surf Process Landf 9:553–565

Vepraskas MJ, Wilding LP, Drees LR (1994) Aquic conditions for soil taxonomy: concepts, soil morphology and micromorphology. In: Ringrose-Voase A, Humphreys G (eds) Soil micromorphology. Elsevier, Amsterdam, pp 117–131

Waltham T (2008) Fengcong, fenglin, cone karst and tower karst. Cave Karst Sci 35:77–88

Wang W-M, Ding J-L, Shu J-W, Chen W (2010) Exploration of early rice farming in China. Quat Int 227:22–28

White WB (2007) Cave sediments and paleoclimate. J Cave Karst Stud 69:76–93

Wu X, Zhang C, Goldberg P, Cohen DJ, Yan P, Arpin T, Bar-Yosef O (2012) Early pottery at 20,000 years ago in Xianrendong cave, China. Science 336:1696–1700

Zhang S (1989) Paleokarst of China. In: Bosak P, Ford D, Glaszek J, Horacek I (eds) Developments in earth surface processes 1: Paleokarst, a systematic and regional review. Elsevier, New York, pp 297–311

Zhang C (1999) The excavations at Xianrendong and Diaotonghuan, Jiangxi. BIPPA 18:97–100

Zhang C (2002) The discovery of early pottery in China. Doc Praehist XXIX:29–35

Zhu XW, Waltham T (2004) Tiankeng: definition and description. Speleogenes Evol Karst Aquifer 4(1):1–8

Zhu X, Zhu D, Zhang Y, Lynch E (2013) Tower karst and cone karst. In: Shroder JF (ed) Treatise on geomorphology. Academic, San Diego, pp 237–340